

Temperature driven false vacuum decay in coherently coupled Bose superfluids

Paniyanchatha Moolayil Sivasankar,^{1,*} Franco Dalfovo,^{2,†} Alessio Recati,^{2,3,‡} and Arko Roy^{1,§}

¹*School of Physical Sciences, Indian Institute of Technology Mandi, Mandi-175075 (H.P.), India*

²*Pitaevskii BEC Center, CNR-INO and Dipartimento di Fisica, Università di Trento, I-38123 Trento, Italy*

³*Trento Institute for Fundamental Physics and Applications, INFN, I-38123 Trento, Italy*

The relaxation of a quantum field from a metastable state (false vacuum) to a stable one (true vacuum), also known as false vacuum decay, is a fundamental problem in quantum field theory and cosmology. We study this phenomenon using a two-dimensional interacting and coherently coupled Bose-Bose mixture, a platform that has already been employed experimentally to investigate false vacuum decay in one dimension. In such a mixture, it is possible to define an effective magnetization that acts as a quantum field variable. Using the Stochastic Gross-Pitaevskii equation (SGPE), we prepare thermal equilibrium states in the false vacuum and extract decay rates from the magnetization dynamics. The decay rates show an exponential dependence on temperature, in line with the thermal theory of instantons. Since the SGPE is based on complex scalar fields, it also allows us to explore the behavior of the phase, which turns out to become dynamic during decay. Our results confirm the SGPE as an effective tool for studying coupled magnetization and phase dynamics and the associated instanton physics in ultracold quantum gases.

I. INTRODUCTION

False vacuum decay (FVD) describes the relaxation of a quantum system from a metastable false vacuum (FV) to a lower-energy true vacuum (TV). In his seminal work, Coleman showed that this transition proceeds via the stochastic nucleation of true vacuum bubbles within the false vacuum background, triggered by quantum fluctuations [1, 2]. Such a decay finds many applications in different areas of science, including early dynamics of our universe [1–6], high-energy physics [7, 8], protein folding [9, 10] and condensed matter systems [11–13]. However, the strongly non-perturbative character of this process has long hindered its direct exploration.

Recent advances in quantum simulation have opened new routes for emulating false vacuum decay in controllable platforms. Proposals for analog realizations range from spin systems [14–20] and digital simulators [21, 22] to ultra-cold atomic gases [23–31], the latter being particularly well suited owing to their isolation from the environment, tunable interactions, and real-time access to non-equilibrium dynamics.

In particular, coherently coupled Bose-Einstein condensates [32] have recently allowed for the experimental observation of false vacuum decay [28, 33]. Despite the apparent simplicity of the system, it hosts many phenomena ranging from internal Josephson dynamics [34–36], quark confinement [37] to magnetism [32, 38]. The system is a gas of atoms dressed by a Rabi coupling between two hyperfine levels that, at low enough temperature, forms a Bose-Einstein condensate with a spinor order parameter. Due to the lack of $SU(2)$ symmetry in the atomic interaction strengths, the system behaves like

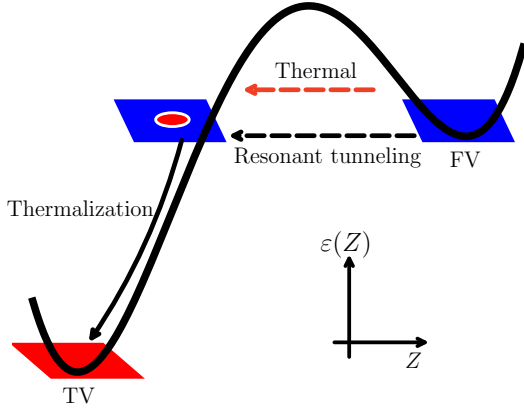


FIG. 1. Schematic illustration of false vacuum decay through the energy landscape. Here ε is the energy and Z is the magnetization. The metastable false vacuum corresponds to the fully polarized $Z = +1$ state on the right (blue plane). It decays by nucleating bubbles (i.e., regions of opposite polarization) which then evolve towards the true vacuum $Z = -1$ state on the left (red plane) through thermalization processes.

an anisotropic ferromagnetic material, and it exhibits a para- to ferromagnetic (easy-axis) transition characterized by the spontaneous \mathbb{Z}_2 ordering of the longitudinal spin component. This transition can be described by the transverse field Ising model and is governed by the ratio between the Rabi coupling and the anisotropy in the intra- and inter-species interaction strengths [38].

In the ferromagnetic phase, the energy landscape as a function of the magnetization (i.e., the relative imbalance of the two components) forms a symmetric double-well potential. This symmetry can be deliberately broken by introducing a finite detuning between the hyperfine levels resonant condition and the oscillating radio-frequency field that couples the two components. This detuning renders the energy landscape an asymmetric double well, as schematically shown in Fig. 1, and it is an experimen-

* ud23002@students.iitmandi.ac.in

† franco.dalfovo@unitn.it

‡ alessio.recati@cnr.it

§ arko@iitmandi.ac.in

tally tunable parameter that can be used to prepare the system under the appropriate conditions to observe false vacuum decay

Theoretical predictions for the decay rate have been obtained in the past by using the instanton theory, corresponding to the imaginary time solutions of the equations of motion of the field [1, 2]. A.D.Linde provided a finite temperature extension of the instanton theory showing that it can greatly enhance the decay rate [39]. Although such a semiclassical picture captures the basic mechanism of FVD, many of the details remain to be verified. Furthermore, the effects of temperature have only been observed experimentally very recently, in a quasi-one-dimensional trapped system [33].

In this work, we use the Stochastic Gross-Pitaevskii formalism to theoretically investigate FVD in a two-dimensional homogeneous system. This theory treats Bose-Einstein condensates at the mean-field level, including temperature effects through fluctuations of a c -field governed by a Gross-Pitaevskii-like equation and coupled to a thermal bath of incoherent atoms [40–42]. In this way, we simulate the FVD process in configurations that are within the reach of state-of-the-art experiments. We qualitatively compare our results with the prediction of finite temperature instanton theory.

The article is organized as follows. In Sec. II we introduce our model system and discuss how it can be used within a stochastic framework to emulate FVD. In Sec. III, we discuss the theory of FVD and present our numerical results.

II. THEORETICAL FRAMEWORK AND INITIAL STATE PREPARATION

A. Zero temperature energy landscape

We consider a dilute, weakly-interacting homogeneous two-component atomic Bose gas in two-dimensions, confined in a square box of area $\mathcal{A} = L_x \times L_y$, with periodic boundary conditions. The two components correspond to atoms in different hyperfine states $|1\rangle$ and $|2\rangle$. An oscillating rf-field of strength Ω , which is detuned from resonance by δ , creates a linear superposition of the two states. By mapping the system to a spin-1/2 model, one can define the magnetization $Z = (N_1 - N_2)/N$, where N_i is the number of atoms in component $i = 1, 2$, and $N = N_1 + N_2$ is the total number. Atoms interact via a two-body contact potential, with intra- and inter-species constants g_{11} , g_{22} , g_{12} . We assume a symmetric mixture with $g_{11} = g_{22} = g$, and define $G = (g + g_{12})/2$ as the density interaction strength, and $\kappa = (g - g_{12})/2$ as the spin interaction strength.

Before addressing the behavior at finite temperature, where the gas is subjected to local fluctuations in density and phase, it is useful to recall what is expected at $T = 0$. In this case, the densities n_1 and n_2 of the two components, as well as the total density $n = n_1 + n_2$,

are constant and the mean-field (grand-canonical) energy density is given by [32, 43]

$$\begin{aligned} \varepsilon(n, Z, \varphi) = & \frac{1}{2}Gn^2 + \frac{1}{2}\kappa n^2 Z^2 - nZ\delta \\ & - \Omega n\sqrt{1 - Z^2} \cos \varphi - \mu n, \end{aligned} \quad (1)$$

where φ is the relative phase of the two components and μ is the chemical potential. The ground state corresponds to $\cos \varphi = 1$ and is obtained by minimizing $\varepsilon(n, Z)$ with respect to Z and n , which yields

$$\begin{aligned} Z\kappa n - \delta + \frac{\Omega Z}{\sqrt{1 - Z^2}} &= 0, \\ \Omega & \\ Gn - \frac{\Omega}{\sqrt{1 - Z^2}} &= \mu. \end{aligned} \quad (2)$$

These equations can be solved numerically by first determining Z and then evaluating μ .

For $\delta = 0$, Eq. (1) describes a degenerate mean-field energy landscape that supports two distinct phases. When $\Omega < |\kappa|n$, the system exhibits a polarized ferromagnetic phase, whereas for $\Omega > |\kappa|n$ it remains in an unpolarized paramagnetic phase. A finite detuning δ breaks the underlying \mathbb{Z}_2 symmetry, resulting a non-degenerate energy landscape. The detuning term energetically biases the minima at $Z \approx \pm 1$ by an amount $2n\delta$, leading to the coexistence of local and global minima.

B. Stochastic Gross-Pitaevskii equation

Given the energy landscape, our goal is to prepare the system at equilibrium in the global free energy minimum at a finite temperature T , then modify the detuning so that the system is transferred into a false vacuum state with thermal fluctuations. For this we use the Stochastic (Projected) Gross-Pitaevskii equation (SGPE)

$$\begin{aligned} i\hbar \frac{\partial \psi_i}{\partial t} = \hat{\mathcal{P}} \left\{ (1 - i\gamma) \left[\left(-\frac{\hbar^2 \nabla^2}{2m} + g|\psi_i|^2 + g_{12}|\psi_{3-i}|^2 \right. \right. \right. \\ \left. \left. \left. + (-1)^i \delta - \mu \right) \psi_i - \Omega \psi_{3-i} \right] + \eta_i \right\}, \end{aligned} \quad (3)$$

which corresponds to the extension to multi-component systems [43–46] of the standard single-component SGPE [40–42]. Here, $\psi_i(\mathbf{x}, t) = \sqrt{n_i(\mathbf{x}, t)} e^{i\phi_i(\mathbf{x}, t)}$ are coherent c -fields in the coordinate space $\mathbf{x} = (x, y)$. The local magnetization is $z(\mathbf{x}, t) = (n_1 - n_2)/(n_1 + n_2)$, while the local relative phase is $\phi(\mathbf{x}, t) = \phi_1 - \phi_2$. The total magnetization coincides with the spatial average of z , as $Z(t) = (1/\mathcal{A}) \int d\mathbf{x} z(\mathbf{x}, t)$, and we define an average relative phase φ such that $\cos \varphi(t) = (1/\mathcal{A}) \int d\mathbf{x} \cos \phi(\mathbf{x}, t)$. The c -fields describe the low-lying macroscopically occupied modes of each components up to a cut-off energy $\epsilon_{\text{cut}} = k_B T \ln(2) + \mu$, where the mean occupation number of single-particle modes is of order 1. The projector

$\hat{\mathcal{P}}$ confines the dynamics to the coherent fields below the cut-off, while higher-energy modes form a thermal reservoir that generates Gaussian noise satisfying the condition

$$\langle \eta_i(\mathbf{x}, t) \eta_j^*(\mathbf{x}', t') \rangle = 2\hbar\gamma k_B T \delta(\mathbf{x} - \mathbf{x}') \delta(t - t') \delta_{ij}, \quad (4)$$

where $\langle \dots \rangle$ denotes the averaging over different noise realizations. Following Refs. [47–49], we assume that the noise term is the same for both components. The dissipation parameter γ couples the coherent region to the incoherent thermal reservoir. Its value affects the thermalization rate, but it does not alter the main properties of the final state after equilibration. Unless otherwise stated, we choose $\gamma = 0.01$. Finally, for convenience, we introduce the temperature scale $T_s = |\kappa|n/k_B$, referred to as the effective spin temperature, to represent T in dimensionless units.

It is worth stressing that, within SGPE, results obtained from independent noise realizations may be regarded consistent with the representation of the outcomes of individual experimental runs (see, e.g., [50–52]). Due to the stochastic nature of the noise, each realization yields different dynamical trajectories, as it is also the case in repeated measurements. However, experiments cannot follow the temporal evolution of individual stochastic trajectories; a measurement at time t simply captures the outcome of one realization within the underlying ensemble of trajectories [28].

C. Initial state preparation

The parameters entering Eq. (3) are chosen to emulate typical experimental conditions [53, 54]. For the computational box we choose $L_x = L_y = 25 \mu\text{m}$. The chemical potential μ , which is an input parameter in (3), is chosen through Eq. (2) so that the total number of atoms in the box is of the order of 10^4 . A natural energy scale is provided by gn , for which we have $gn/k_B = 8.5 \text{ nK}$. For the mass we take $mg/\hbar^2 = 0.095$. The coherent coupling is chosen as $\Omega = 0.03 gn$, within the range accessible to current experiments [36, 55]. We finally take $g_{12} = 1.2g$ and an initial detuning $\delta_i = 0.5\Omega$. With these parameters, the effective spin temperature becomes $T_s = 0.1gn/k_B$. The highest absolute temperatures in our simulations are $\sim 7 \text{ nK}$, which are lower than those typically reported in standard BEC experiments. This originates from the relatively low atom numbers (and hence low densities) chosen for our numerical simulations. However, the physically relevant parameter is the ratio between thermal and interaction energy; this implies that mixtures with higher density, within experimentally accessible regimes, will exhibit a similar behavior at larger temperatures.

Equilibrium configurations at a given temperature T and detuning δ_i are obtained by numerically propagating Eq. (3) in real time from random initial c -fields until equilibration. In the SGPE framework, the total number

of atoms is not a direct input; rather, it evolves dynamically during simulations and stabilizes around a steady mean value with small residual fluctuations once equilibrium is reached. We use this stabilization criterion to identify equilibrium states.

After preparing the initial equilibrium state at the global minimum of the energy density (1), the next task is to engineer the false vacuum state. To this end, we follow the experimental ramping protocol of Ref. [28], wherein the detuning is linearly varied from δ_i to the final value δ_f using $\delta(t) = \delta_i - (\delta_i - \delta_f)(1 - t/\tau_r)$, with the chemical potential μ being consistently corrected using Eqs. (2) and (3). The time $\tau_r = -1.6 \text{ (s)}$ sets the beginning of the ramp, which guides the system, almost adiabatically, towards the FV state, i.e., the local minimum of the effective energy landscape, as in Fig. 2 (B). Although the fluctuation–dissipation theorem built into Eq. (3) should ensure that the initial state relaxes into the FV, in practice some trajectories may prematurely decay during the ramping process, especially at high temperatures. Given that our focus is on the decay of FV states, for the subsequent analysis, we restrict our attention to trajectories that have not decayed prematurely. In practice, we select the FV states for which $Z > 0.2$ at the end of the ramping stage ($t = 0$). We have checked that the results for the decay rates remain robust to the precise value of this threshold, provided that it corresponds to a positive magnetization.

III. THE DECAY OF THE FALSE VACUUM

Once a metastable FV state is successfully prepared, we switch off the dissipation parameter γ in (3) and evolve the system under the resulting conservative projected Gross–Pitaevskii equation (PGPE). Setting $\gamma = 0$ at this stage, ensures that the decay process is not affected by spurious processes caused by atom losses in the non-conservative SGPE, while keeping the relevant effects of thermal fluctuations within the c -fields. If $\gamma \neq 0$, the dynamics would acquire an additional time scale that hinders the intrinsic FVD mechanism, causing the observed decay to explicitly depend on γ . The same protocol has already been used in similar cases as, for instance, for the investigation of sound propagation in 2D condensates [46, 54].

The ensuing dynamics of the magnetization density reveals the decay of the FV towards the TV, which is characterized by the appearance and growth of bubbles of atoms of opposite polarization, as shown in Fig. 2 (a)–(i). This is consistent with the semiclassical instanton picture, where decay occurs *via* the nucleation of resonant bubbles, which are formed when the energy gain from the bulk is balanced by the surface energy of the bubble walls [1, 2]. The nucleation probability per unit time and area is characterized by the decay rate Γ , which quantifies the transition of the false vacuum into a bubble configuration. Unlike single-particle tunneling, the

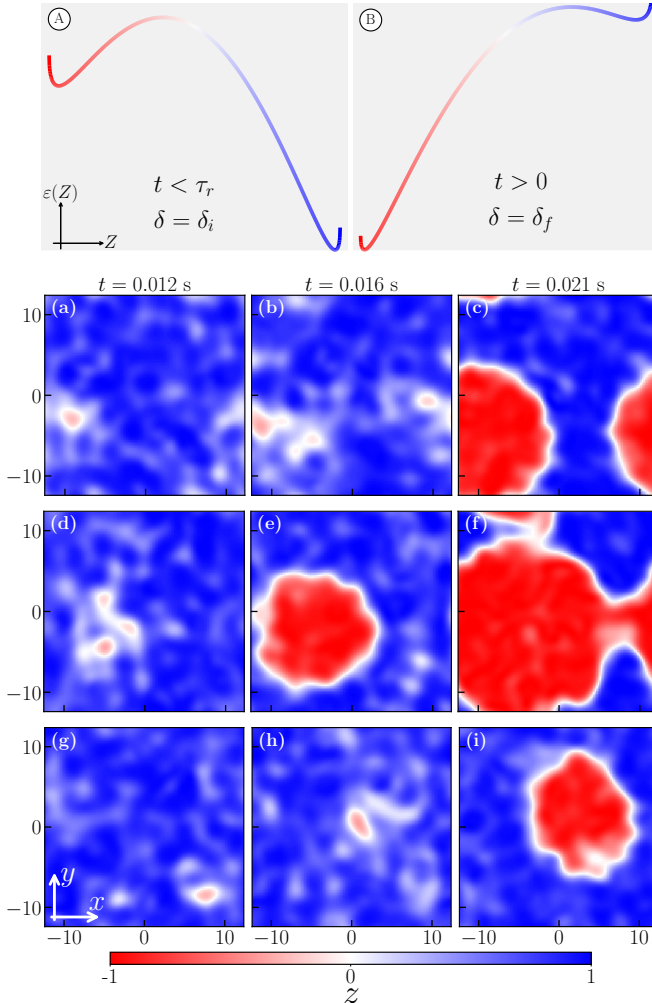


FIG. 2. Panels ① and ② show the energy landscapes, in arbitrary units, described by Eq. (1). In ①, for an initial positive detuning $\delta_i = 0.5\Omega$, the system is prepared at equilibrium near the global minimum ($Z \approx 1$) at temperature $T = 5.5T_s$. For $\tau_r < t < 0$, with $\tau_r = -1.6$ s, the detuning is linearly varied from the initial δ_i to a final negative value $\delta_f = -1.0\Omega$, hence transferring the system into a metastable state, as in ②. The system subsequently decays into the true vacuum. Panels (a)–(i) show typical snapshots of the local magnetization $z = (n_1 - n_2)/(n_1 + n_2)$ in the $x-y$ plane at three different times during the decay process, namely 12, 16 and 21 ms. Each square box has length 25 μm and periodic boundary conditions. Each row corresponds to a distinct stochastic noise realization. The figure shows bubbles of condensate 2 (red) forming and growing in condensate 1 (blue).

decay rate in field theory exhibits a nontrivial dependence on the barrier parameters, which in our system are controlled by the externally tunable parameters δ and Ω . At finite temperatures, Linde's extension of instanton theory shows that decay can proceed from thermally excited states, with the total rate obtained by summing over these contributions weighted by a Boltzmann fac-

tor [39, 56]. The decay rate takes the form

$$\Gamma = A e^{-\beta E_c}, \quad (5)$$

where E_c is the critical instanton energy and $\beta = 1/k_B T$. The prefactor A captures the fluctuations around the critical bubble and depends on the underlying system parameters; its temperature dependence is assumed to be weak compared to that of the exponential term. For a one-dimensional geometry, in very specific regimes, analytical results for E_c and A can be obtained [28, 57]. For our two-dimensional configuration there are no available results and in the following we treat them as fitting parameters.

Linde's finite-temperature framework applies when thermal fluctuations dominate over quantum fluctuations ($T \gg T_s$) while still satisfying $k_B T \ll E_c$. For $k_B T \gg E_c$, the system simply rolls down the barrier without tunneling. In our numerical investigations we set the thermal energy $k_B T$ to be much lesser than the many-body energy associated with the barrier height described by Eq. (1). It should, however, be emphasized that E_c is not merely the energy of the barrier height, but the energy of the critical bubble configuration, for which there are no analytical predictions; its determination is beyond the scope of the current work.

In our numerical simulations, the dynamics can be analyzed in terms of both density and spin channels, which correspond to the in-phase and out-of phase modes, respectively. Within a hydrodynamic-like formalism, the system is usually described in terms of the local variables n , z and ϕ , where the density n evolves according to the continuity equation, the magnetization z is determined by the spin sector of the energy density, and the relative phase ϕ obeys an Euler-type equation [32]. In the presence of a weak Rabi coupling ($\Omega \ll \mu$), as in our case, and for $g_{12} \approx g$, the density channel is weakly affected by the perturbations in the spin channel. Consequently, the relevant variables of the system reduce to those of magnetization channel, i.e., magnetization and relative phase, which obey coupled Josephson equations [32]. Since z and ϕ are canonically conjugate variables, they are intrinsically coupled and cannot be treated independently. The false vacuum state is therefore naturally described by a complex scalar field in which both degrees of freedom play an essential role in the process. In the following, we analyze the results of our numerical simulations, focusing first on the decay dynamics of the magnetization and then examining the associated dynamics of the relative phase.

A. Magnetization trajectories and survival probability

To study the real-time dynamics of the decay process, we evolve the post-ramp state using the PGPE and monitor the behavior of the global magnetization

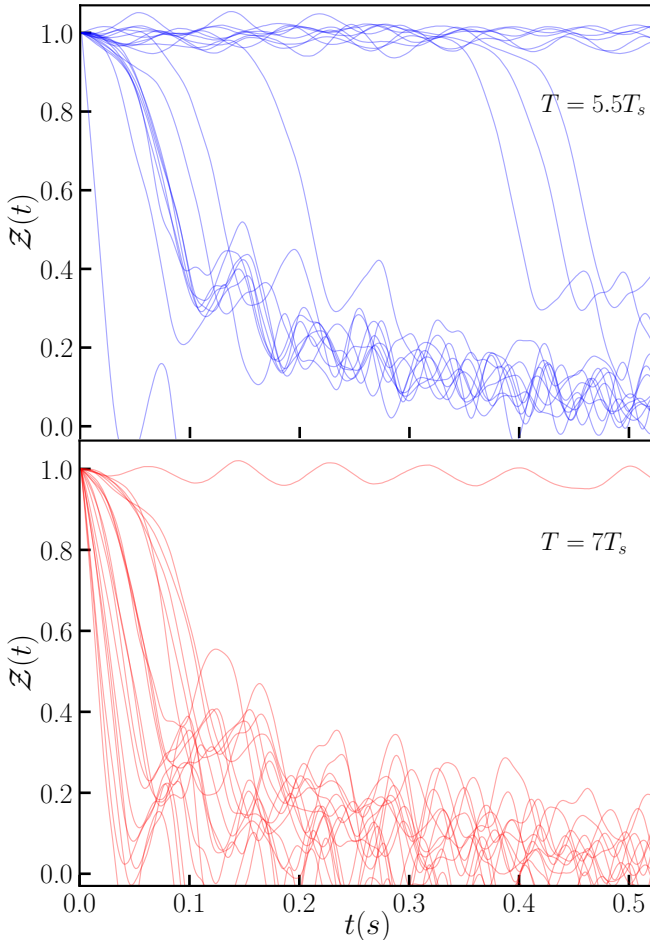


FIG. 3. Representative trajectories of the rescaled magnetization $\mathcal{Z}(t)$ obtained by solving the PGPE from 20 different stochastic realizations and two different temperatures. Here the detuning is $\delta_f = -\Omega$. The false vacuum decay occurs when $\mathcal{Z}(t)$ exhibits a sharp decrease, corresponding to the growth of bubbles with $Z \approx -1$ (true vacuum) in a medium with $Z \approx 1$ (false vacuum). The variation in decay times reflects the intrinsic stochasticity of the process. At $T = 7T_s$, the trajectories exhibit a narrower spread and decay rapidly, whereas at $T = 5.5T_s$ the decay occurs slowly with greater variability.

$Z(t)$. In order to quantify the decay rate, it is convenient to introduce the rescaled magnetization $\mathcal{Z}(t) = (1/2)(1 + Z(t)/Z(0))$ and follow its time evolution for each noise realization at a given temperature. Examples are shown in Fig. 3 for 20 noise realizations at $T = 5.5T_s$ (upper panel), and the same number at $7T_s$ (lower panel). We typically collect trajectories for $\mathcal{N} = 100$ different noise realizations at each temperature, and repeat it for different temperatures. The lowest temperature used in the simulations is selected to ensure sufficient decay statistics for estimating Γ , while the highest temperature ($T = 8T_s$) is constrained by the prevalence of premature decays and is approximately $0.1T_{\text{BKT}}$, where T_{BKT} is the critical temperature of the Kosterlitz-Berezinskii

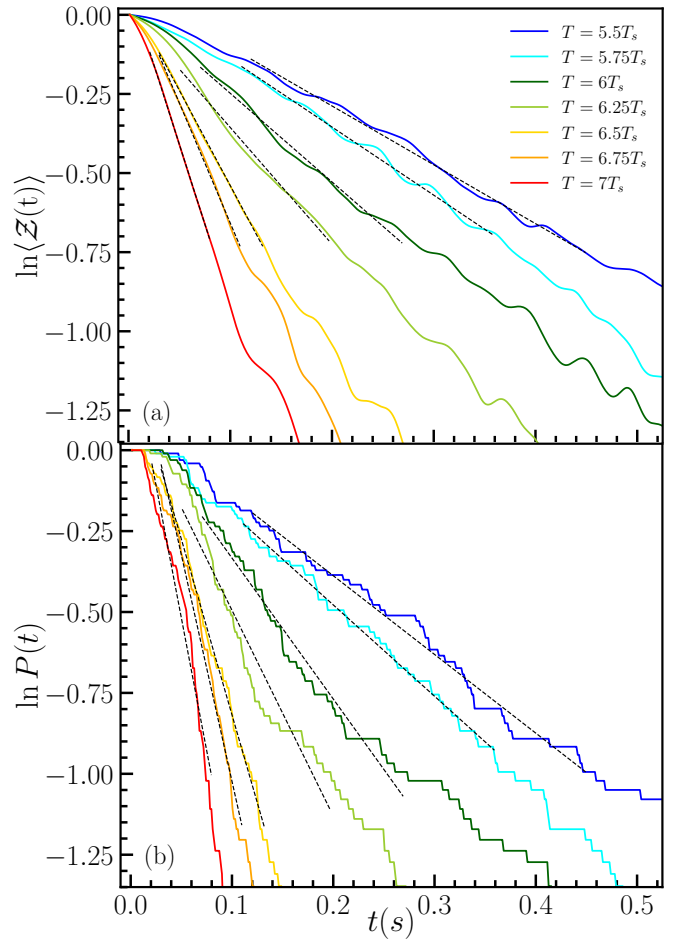


FIG. 4. Logarithm of survival probability *vs.* time, at various temperatures and for $\delta_f = -\Omega$. In (a) the survival probability is defined as the ensemble average of the rescaled magnetization, while in (b) is obtained by counting the number $P(t)$ of trajectories which are not yet decayed at time t . All curves clearly exhibit exponential behavior, with both $\langle \mathcal{Z}(t) \rangle$ and $P(t)$ being proportional to $e^{-\Gamma t}$. The black dashed lines correspond to the fitting functions used to extract the decay rate Γ . For each temperature, the time interval used for the fit starts approximately when the first growing bubble appears and ends when the true vacuum occupies about half of the box.

Thouless transition for a single component Bose gas in the 2D geometry [58].

As expected, most of the trajectories shown in Fig. 3 exhibit a sharp decrease from $\mathcal{Z} = 1$ (false vacuum) towards $\mathcal{Z} \approx 0$ (true vacuum), but this decay occurs at different times depending on the initial noise. Also, the decay is systematically faster at higher temperature. From these trajectories, one can define a *survival probability* in two different ways. The first consists of computing the ensemble average of the rescaled magnetization, $\langle \mathcal{Z}(t) \rangle$, over \mathcal{N} noise realizations, which is expected to follow an exponential law [28, 59]. The interpretation of this quantity as the *survival probability* is not straightforward, since it involves an average over both surviv-

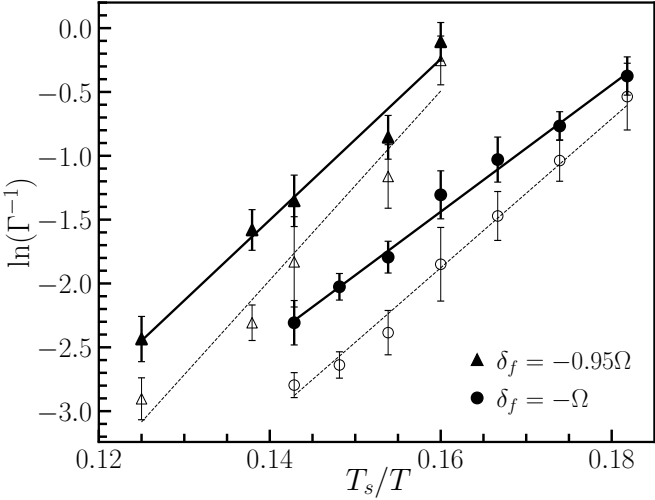


FIG. 5. Temperature dependence of the decay rate Γ , extracted for $\delta_f = -\Omega$ and $\delta_f = -0.95\Omega$. The solid and empty markers represent the decay rate obtained from Fig. 4(a) and (b), respectively. The vertical error bars denote the statistical uncertainties in the estimated decay rates, obtained via the bootstrapping procedure [61, 62]. The numerical data exhibit excellent agreement with the instanton prediction, $\Gamma \propto e^{-\beta E_c}$. For $\delta_f = -0.95\Omega$, the higher potential barrier leads to a reduced decay rate at any given temperature. The straight lines are the fitted curves to the data represented through the markers.

ing and decayed trajectories. Consequently, it also captures contributions from post bubble nucleation dynamics such as growth, expansion and thermalization into the true vacuum. The second consists of counting the fraction $P(t)$ of trajectories that remain in the false vacuum for a time t , i.e., those with $Z(t) > 0$ (or equivalently $\mathcal{Z}(t) > 0.5$). This quantity has a direct probabilistic interpretation and is expected to exhibit exponential decay in time, thereby providing an alternative estimate of the survival probability [60], that is less affected by the post-nucleation dynamics. Our results for both protocols are shown in Fig. 4 in log-scale. In the long-time limit, all curves eventually decay, leading both $\langle \mathcal{Z}(t) \rangle$ and $P(t)$ to vanish. The stepwise behavior of $P(t)$, which is visible in Fig. 4(b), reflects the character of the counting procedure, which includes time intervals during which no decay events occur within our *ensemble* of trajectories.

B. Decay rate

The decay rate is extracted by fitting the curves of $\langle \mathcal{Z}(t) \rangle$ and $P(t)$ in a temporal window in which both exhibit a clear exponential decay [25, 63] (see Fig. 4). In particular, the function $\ln \langle \mathcal{Z}(t) \rangle = \ln A_Z - \Gamma t$ provides an excellent fit to the data for $\langle \mathcal{Z}(t) \rangle$ in the interval $[0.5, 0.9]$, with both A_Z and Γ treated as fitting parameters. Within this temporal range, the cumulative bubble area remains below half of the system size,

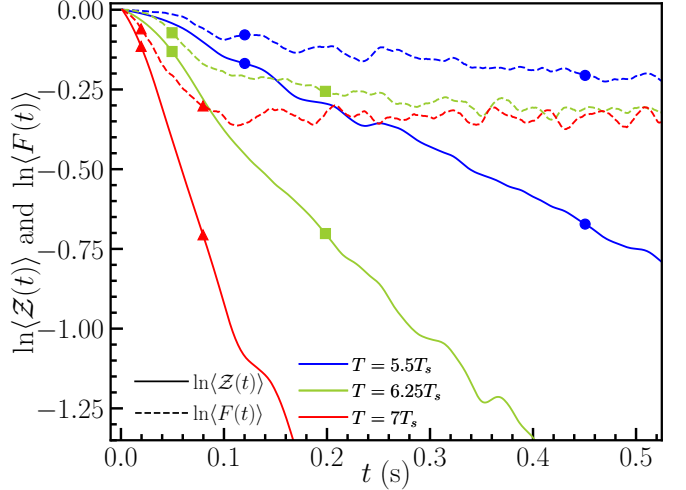


FIG. 6. Magnetization and relative phase dynamics for three different temperatures. The three solid curves are the same as in Fig. 4(a) for the selected values of T , and represent the logarithm of the ensemble average of the rescaled magnetization. The dashed lines represent the logarithm of the ensemble average of the rescaled $\cos \varphi$, where φ is the relative phase. The ensemble average is computed over $\mathcal{N} = 100$ noise realizations. For each line, a pair of markers delimits the time window used for the linear fit in Fig. 4

thereby avoiding significant finite-size effects. We repeat the fitting procedure also for $P(t)$ in the same temporal window, with the function $\ln P(t) = \ln A_P - \Gamma t$, again treating A_P and Γ as fitting parameters. Our numerical results for the decay rate Γ are reported in Fig. 5 for two values of the detuning δ_f . The filled black markers are derived from $\langle \mathcal{Z}(t) \rangle$ (first protocol), while the empty markers from $P(t)$ (second protocol), with circles and triangles denoting the different detuning. The error bars account for the effects of ensemble averaging and are estimated via a bootstrapping procedure [61, 62]. In the figure, we actually plot the function $\ln(\Gamma^{-1})$ vs. T_s/T . The resulting linear dependence is consistent with the predictions of the instanton theory, expressed by Eq. (5). The slope can therefore be identified as the critical instanton energy, E_c/k_B . From the first protocol (thick solid black lines), for $\delta_f = -\Omega$, we obtain $E_c/k_B = (50 \pm 4)$ nK and for $\delta_f = -0.95\Omega$, we find $E_c/k_B = (63 \pm 6)$ nK. From the second protocol (thin dashed lines), the corresponding slopes yield (58 ± 5) nK and (74 ± 7) nK, respectively. In all cases, uncertainties are estimated from the linear fit. Although the numerical values of Γ extracted from the two protocols are not identical, they both clearly show the expected exponential dependence on temperature. Furthermore, the linearity of the data indicates that, within the temperature values considered, E_c remains temperature-independent. As expected, the slope, E_c/k_B becomes larger for larger barrier height from both protocols. The positive slope reflects the enhancement of the decay rate with temperature, consistent with the thermal instanton theory.

C. Relative phase dynamics

In PGPE simulations, we can also monitor the temporal evolution of the relative phase, as defined in Section II B. In non-equilibrium processes, such as false vacuum decay, the relative phase φ can take any values in the range $[-\pi, \pi]$. Since the energy depends on $\cos \varphi$, configurations with $\pm \varphi$ are energetically identical, leading to the occurrence of solutions exhibiting both configurations. This naturally motivates an estimate of the weight of the $\cos \varphi$ contribution in the energy landscape, Eq. (1). In [28, 33, 57], it is assumed that the relative phase is locked during decay, so that the energy landscape is determined only by magnetization Z . Here we find that the relative phase actually evolves. To prove it, as we have already done for $Z(t)$, we introduce a rescaled function $F(t) = (1/2)(1 + \cos \varphi(t)/\cos \varphi(0))$ and average it over many noise realizations. In Fig. 6, the temporal evolution $\langle F(t) \rangle$ is compared with the one of $\langle Z(t) \rangle$. The figure shows that, as the magnetization decays toward true vacuum (i.e., $\langle Z \rangle \rightarrow 0$), the phase also changes, relaxing toward a constant value that shows only a weak dependence on temperature. Most of its variation occurs in relatively short times. The overall variation is not large, but it can significantly affect how the system crosses the barrier in the energy landscape. By inserting the ensemble averages of $Z(t)$ and $\cos \varphi(t)$ into (1), we find that the energy values at the extremes of the time window used to extract the decay rates are comparable and that the energy has its maximum within the same interval. This indicates that the initial variation in the relative phase is relevant for ensuring the conditions for resonant bubble nucleation. It also emphasizes the importance of using complex scalar fields in the description of coherently coupled Bose superfluids such that Z and φ are treated on equal footing, thus allowing a better understanding of the instanton physics.

IV. CONCLUSIONS

We have investigated finite-temperature false vacuum decay in coherently coupled two-dimensional homogeneous Bose–Einstein condensates, employing the

Stochastic Gross-Pitaevskii formalism to prepare thermal false-vacuum states and track their decay through global magnetization dynamics. Our analysis shows that the decay rate exhibits an exponential dependence on temperature, $\Gamma \propto e^{-\beta E_c}$, in agreement with thermal instanton theory. Furthermore, we elucidate the dynamics of the relative phase and suggest the need to develop an instanton theory describing a complex scalar field considering both magnetization and relative phase as relevant degrees of freedom, such as in coherently coupled Bose–Bose mixtures.

Our study places ultracold atoms as a viable platform to probe field-theoretic phenomena like vacuum decay, with the possibility of near-term experimental validation. Given the high computational cost of large-scale SGPE simulations, our present study is restricted to a given system size; a systematic exploration of barrier scaling and finite-size effects remains an important direction for further study. Finally, while we have noted that false vacuum decay shares qualitative features with the Kramers escape problem [64], in particular an exponential dependence of the decay rate in the thermally dominated regime, a field-theoretical analysis is needed to clarify their fundamental differences, and the development of such an analysis constitutes a promising avenue for subsequent research.

ACKNOWLEDGMENTS

We thank Subhadeep Patra and Sunilkumar Venkateshappa for several insightful discussions. Sivasankar gratefully acknowledges M. Obasho for constructive discussions on GPU-based implementation. A. Roy acknowledges the support of the Science and Engineering Research Board (SERB), Department of Science and Technology, Government of India, under the project SRG/2022/000057 and IIT Mandi seed-grant funds under the project IITM/SG/AR/87. A. Roy acknowledges the National Supercomputing Mission (NSM) for providing computing resources of PARAM Himalaya at IIT Mandi, which is implemented by C-DAC and supported by the Ministry of Electronics and Information Technology (MeitY) and Department of Science and Technology (DST), Government of India. F. Dalfovo and A. Recati thank the Provincia autonoma di Trento for support.

[1] S. Coleman, Fate of the false vacuum: Semiclassical theory, *Phys. Rev. D* **15**, 2929 (1977).

[2] C. G. Callan and S. Coleman, Fate of the false vacuum. ii. first quantum corrections, *Phys. Rev. D* **16**, 1762 (1977).

[3] I. Y. Kobzarev, L. B. Okun, and M. B. Voloshin, Bubbles in metastable vacuum, *Yad. Fiz.* **20**, 1229 (1974).

[4] S. Coleman and F. De Luccia, Gravitational effects on and of vacuum decay, *Phys. Rev. D* **21**, 3305 (1980).

[5] M. Hindmarsh, M. Lüben, J. Lumma, and M. Pauly, Phase transitions in the early universe, *SciPost Phys. Lect. Notes* , 24 (2021).

[6] P. Burda, R. Gregory, and I. G. Moss, Gravity and the stability of the Higgs vacuum, *Phys. Rev. Lett.* **115**, 071303 (2015).

[7] M. Stone, Semiclassical methods for unstable states, *Phys. Lett. B* **67**, 186 (1977).

[8] M. E. Shaposhnikov, Baryon asymmetry of the universe in standard electroweak theory, *Nucl. Phys. B* **287**, 757

(1987).

[9] A. J. Baldwin, T. P. J. Knowles, G. G. Tartaglia, A. W. Fitzpatrick, G. L. Devlin, S. L. Shammas, C. A. Waudby, M. F. Mossuto, S. Meehan, S. L. Gras, J. Christodoulou, S. J. Anthony-Cahill, P. D. Barker, M. Vendruscolo, and C. M. Dobson, Metastability of native proteins and the phenomenon of amyloid formation, *J. Am. Chem. Soc.* **133**, 14160 (2011).

[10] D. K. Ghosh and A. Ranjan, The metastable states of proteins, *Protein Sci.* **29**, 1559 (2020).

[11] D. W. Oxtoby, Homogeneous nucleation: theory and experiment, *J. Phys.: Condens. Matter* **4**, 7627 (1992).

[12] P. G. Debenedetti and F. H. Stillinger, Supercooled liquids and the glass transition, *Nature* **410**, 259 (2001).

[13] R. Coldea, D. A. Tennant, E. M. Wheeler, E. Wawrzynska, D. Prabhakaran, M. Telling, K. Habicht, P. Smeibidl, and K. Kiefer, Quantum criticality in an Ising chain: Experimental evidence for emergent E_8 symmetry, *Science* **327**, 177 (2010).

[14] S. B. Rutkevich, Decay of the metastable phase in $d = 1$ and $d = 2$ Ising models, *Phys. Rev. B* **60**, 14525 (1999).

[15] A. Sinha, T. Chanda, and J. Dziarmaga, Nonadiabatic dynamics across a first-order quantum phase transition: Quantized bubble nucleation, *Phys. Rev. B* **103**, L220302 (2021).

[16] G. Lagnese, F. M. Surace, S. Morampudi, and F. Wilczek, Detecting a long-lived false vacuum with quantum quenches, *Phys. Rev. Lett.* **133**, 240402 (2024).

[17] C. Johansen, A. Recati, I. Carusotto, and A. Biella, Many-body theory of false vacuum decay in quantum spin chains (2025), [arXiv:2508.13780](https://arxiv.org/abs/2508.13780).

[18] L. Pavešić, M. Di Liberto, and S. Montangero, Scattering and induced false vacuum decay in the two-dimensional quantum Ising model (2025), [arXiv:2509.02702](https://arxiv.org/abs/2509.02702).

[19] D. Maertens, J. Haegeman, and K. Van Acoleyen, Real-time bubble nucleation and growth for false vacuum decay on the lattice (2025), [arXiv:2508.13645](https://arxiv.org/abs/2508.13645).

[20] U. Borla, A. Lazarides, C. Groß, and J. C. Halimeh, Microscopic Dynamics of False Vacuum Decay in the 2+1D Quantum Ising Model (2026), [arXiv:2601.04305](https://arxiv.org/abs/2601.04305).

[21] S. Abel and M. Spannowsky, Quantum-field-theoretic simulation platform for observing the fate of the false vacuum, *PRX Quantum* **2**, 010349 (2021).

[22] J. Vodeb, J.-Y. Desaules, A. Hallam, A. Rava, G. Humar, D. Willsch, F. Jin, M. Willsch, K. Michielsen, and Z. Papić, Stirring the false vacuum via interacting quantized bubbles on a 5,564-qubit quantum annealer, *Nat. Phys.* **21**, 386 (2025).

[23] O. Fialko, B. Opanchuk, A. I. Sidorov, P. D. Drummond, and J. Brand, The universe on a table top: Engineering quantum decay of a relativistic scalar field from a metastable vacuum, *J. Phys. B* **50**, 024003 (2017).

[24] J. Braden, M. C. Johnson, H. V. Peiris, and S. Weinfurter, Towards the cold atom analog false vacuum, *J. High Energy Phys.* **07**, 014.

[25] T. P. Billam, K. Brown, and I. G. Moss, Simulating cosmological supercooling with a cold-atom system, *Phys. Rev. A* **102**, 043324 (2020).

[26] T. P. Billam, K. Brown, A. J. Groszek, and I. G. Moss, Simulating cosmological supercooling with a cold atom system. ii. thermal damping and parametric instability, *Phys. Rev. A* **104**, 053309 (2021).

[27] T. P. Billam, K. Brown, and I. G. Moss, False-vacuum decay in an ultracold spin-1 Bose gas, *Phys. Rev. A* **105**, L041301 (2022).

[28] A. Zenesini, A. Berti, R. Cominotti, C. Rogora, I. G. Moss, T. P. Billam, I. Carusotto, G. Lamporesi, A. Recati, and G. Ferrari, False vacuum decay via bubble formation in ferromagnetic superfluids, *Nat. Phys.* **20**, 558 (2024).

[29] S. Darbha, M. Kornjača, F. Liu, J. Balewski, M. R. Hirsbrunner, P. L. S. Lopes, S.-T. Wang, R. Van Beeumen, D. Camps, and K. Klymko, False vacuum decay and nucleation dynamics in neutral atom systems, *Phys. Rev. B* **110**, 155103 (2024).

[30] K. Brown, I. G. Moss, and T. P. Billam, Mitigating boundary effects in finite temperature simulations of false vacuum decay (2025), [arXiv:2504.03509](https://arxiv.org/abs/2504.03509).

[31] A. C. Jenkins, H. V. Peiris, and A. Pontzen, Bubbles in a box: Eliminating edge nucleation in cold-atom simulators of vacuum decay, *Phys. Rev. A* **112**, 023318 (2025).

[32] A. Recati and S. Stringari, Coherently coupled mixtures of ultracold atomic gases, *Annu. Rev. Condens. Matter Phys.* **13**, 407 (2022).

[33] R. Cominotti, C. Baroni, C. Rogora, D. Andreoni, G. Guarda, G. Lamporesi, G. Ferrari, and A. Zenesini, Observation of temperature effects on false vacuum decay in atomic quantum gases, *Phys. Rev. Lett.* **135**, 183401 (2025).

[34] T. Zibold, E. Nicklas, C. Gross, and M. K. Oberthaler, Classical bifurcation at the transition from Rabi to Josephson dynamics, *Phys. Rev. Lett.* **105**, 204101 (2010).

[35] A. Farolfi, A. Zenesini, D. Trypogeorgos, C. Mordini, A. Gallemí, A. Roy, A. Recati, G. Lamporesi, and G. Ferrari, Quantum-torque-induced breaking of magnetic interfaces in ultracold gases, *Nat. Phys.* **17**, 1359 (2021).

[36] A. Farolfi, A. Zenesini, R. Cominotti, D. Trypogeorgos, A. Recati, G. Lamporesi, and G. Ferrari, Manipulation of an elongated internal Josephson junction of bosonic atoms, *Phys. Rev. A* **104**, 023326 (2021).

[37] M. Eto and M. Nitta, Confinement of half-quantized vortices in coherently coupled Bose-Einstein condensates: Simulating quark confinement in a qcd-like theory, *Phys. Rev. A* **97**, 023613 (2018).

[38] R. Cominotti, A. Berti, C. Dulin, C. Rogora, G. Lamporesi, I. Carusotto, A. Recati, A. Zenesini, and G. Ferrari, Ferromagnetism in an extended coherently coupled atomic superfluid, *Phys. Rev. X* **13**, 021037 (2023).

[39] A. D. Linde, Decay of the false vacuum at finite temperature, *Nucl. Phys. B* **216**, 421 (1983), [Erratum: Nucl. Phys. B 223, 544 (1983)].

[40] H. T. C. Stoof and M. J. Bijlsma, Dynamics of fluctuating Bose-Einstein condensates, *J. Low Temp. Phys.* **124**, 431 (2001).

[41] N. P. Proukakis and B. Jackson, Finite-temperature models of Bose-Einstein condensation, *J. Phys. B: At. Mol. Opt. Phys.* **41**, 203002 (2008).

[42] P. B. Blakie, A. S. Bradley, M. J. Davis, R. J. Ballagh, and C. W. Gardiner, Dynamics and statistical mechanics of ultra-cold Bose gases using c-field techniques, *Adv. Phys.* **57**, 363 (2008).

[43] A. Roy, M. Ota, F. Dalfovo, and A. Recati, Finite-temperature ferromagnetic transition in coherently coupled Bose gases, *Phys. Rev. A* **107**, 043301 (2023).

[44] A. S. Bradley and P. B. Blakie, Stochastic projected Gross-Pitaevskii equation for spinor and multicomponent condensates, *Phys. Rev. A* **90**, 023631 (2014).

[45] M. Ota, F. Larcher, F. Dalfovo, L. Pitaevskii, N. P. Proukakis, and S. Stringari, Collisionless sound in a uniform two-dimensional Bose gas, *Phys. Rev. Lett.* **121**, 145302 (2018).

[46] A. Roy, M. Ota, A. Recati, and F. Dalfovo, Finite-temperature spin dynamics of a two-dimensional Bose-Bose atomic mixture, *Phys. Rev. Res.* **3**, 013161 (2021).

[47] C.-F. Liu, H. Fan, Y.-C. Zhang, D.-S. Wang, and W.-M. Liu, Circular-hyperbolic skyrmion in rotating pseudo-spin-1/2 Bose-Einstein condensates with spin-orbit coupling, *Phys. Rev. A* **86**, 053616 (2012).

[48] S.-W. Su, I.-K. Liu, Y.-C. Tsai, W. M. Liu, and S.-C. Gou, Crystallized half-skyrmions and inverted half-skyrmions in the condensation of spin-1 Bose gases with spin-orbit coupling, *Phys. Rev. A* **86**, 023601 (2012).

[49] S.-W. Su, I.-K. Liu, S.-C. Gou, R. Liao, O. Fialko, and J. Brand, Hidden long-range order in a spin-orbit-coupled two-dimensional Bose gas, *Phys. Rev. A* **95**, 053629 (2017).

[50] K. Sakmann and M. Kasevich, Single-shot simulations of dynamic quantum many-body systems, *Nat. Phys.* **12**, 451 (2016).

[51] K. Sakmann and M. Kasevich, Reply to the correspondence of Drummond and Brand [arxiv:1610.07633] (2017), [arXiv:1702.01211](https://arxiv.org/abs/1702.01211).

[52] M. K. Olsen, J. F. Corney, R. J. Lewis-Swan, and A. S. Bradley, Correspondence on “Single-shot simulations of dynamic quantum many-body systems” (2017), [arXiv:1702.00282](https://arxiv.org/abs/1702.00282).

[53] A. L. Gaunt, T. F. Schmidutz, I. Gotlibovych, R. P. Smith, and Z. Hadzibabic, Bose-Einstein condensation of atoms in a uniform potential, *Phys. Rev. Lett.* **110**, 200406 (2013).

[54] J. L. Ville, R. Saint-Jalm, E. Le Cerf, M. Aidelsburger, S. Nascimbène, J. Dalibard, and J. Beugnon, Sound propagation in a uniform superfluid two-dimensional Bose gas, *Phys. Rev. Lett.* **121**, 145301 (2018).

[55] R. Cominotti, A. Berti, A. Farolfi, A. Zenesini, G. Lamporesi, I. Carusotto, A. Recati, and G. Ferrari, Observation of massless and massive collective excitations with Faraday patterns in a two-component superfluid, *Phys. Rev. Lett.* **128**, 210401 (2022).

[56] I. Affleck, Quantum-statistical metastability, *Phys. Rev. Lett.* **46**, 388 (1981).

[57] E. R. Garcia and J. Hofmann, Instanton theory and fluctuation corrections to the thermal nucleation rate of a ferromagnetic superfluid (2026), [arXiv:2512.20734](https://arxiv.org/abs/2512.20734).

[58] N. Prokof'ev, O. Ruebenacker, and B. Svistunov, Critical point of a weakly interacting two-dimensional Bose gas, *Phys. Rev. Lett.* **87**, 270402 (2001).

[59] G. Lagnese, F. M. Surace, M. Kormos, and P. Calabrese, False vacuum decay in quantum spin chains, *Phys. Rev. B* **104**, L201106 (2021).

[60] D. Pîrvu, A. Shkerin, and S. Sibiryakov, Thermal false vacuum decay in (1+1)-dimensions: Evidence for non-equilibrium dynamics (2024), [arXiv:2408.06411](https://arxiv.org/abs/2408.06411).

[61] T. P. Billam, R. Gregory, F. Michel, and I. G. Moss, Simulating seeded vacuum decay in a cold atom system, *Phys. Rev. D* **100**, 065016 (2019).

[62] The decay rate, Γ is extracted from the survival probability $\langle \mathcal{Z}(t) \rangle$, after averaging over individual stochastic realizations. This prevents a direct access to the intrinsic statistical distribution of Γ . Bootstrapping provides a way to estimate the uncertainty of the intrinsic distribution from the existing dataset ($N = 100$) without generating additional data. From the original 100 trajectories, we construct 10,000 bootstrapped samples. For each bootstrapped sample, 100 trajectories are drawn with replacement, and Γ is computed by exponential fitting in the range $\langle \mathcal{Z}(t) \rangle \in [0.5, 0.9]$ as shown in the main text. The resulting standard deviation of the distribution of Γ across the bootstrapped samples yield error bars for each temperature. An identical bootstrapping protocol is adopted to estimate the errorbars in the decay rates extracted from $P(t)$.

[63] D. Szász-Schagrin and G. Takács, False vacuum decay in the (1+1)-dimensional φ^4 theory, *Phys. Rev. D* **106**, 025008 (2022).

[64] A. Berera, J. Mabillard, B. W. Mintz, and R. O. Ramos, Formulating the Kramers problem in field theory, *Phys. Rev. D* **100**, 076005 (2019).